ACS Catalysis

Research Article

pubs.acs.org/acscatalysis

Correlations among Structure, Electronic Properties, and Photochemical Water Oxidation: A Case Study on Lithium Cobalt Oxides

Hongfei Liu,[†] Ying Zhou,[‡] René Moré,[†] Rafael Müller,[†] Thomas Fox,[†] and Greta R. Patzke*[,†]

[†]Department of Chemistry, University of Zurich, Winterthurerstrasse 190, CH-8057 Zurich, Switzerland

[‡]State Key Laboratory of Oil and Gas Reservoir Geology and Exploitation, School of Materials Science and Engineering, Southwest Petroleum University, Chengdu 610500, People's Republic of China

Supporting Information

ABSTRACT: Construction of $\{M_4O_4\}$ motifs is an effective design paradigm for molecular polyoxometalate- and oxide-based water oxidation catalysts (WOCs). However, the mechanisms beneath this bioinspired design strategy remain a topic of intense debate. The two modifications of $LiCoO_2$ with spinel-type and layer structures are exceptionally versatile model systems to explore the correlations among structure, electronic properties, and photochemical water oxidation. The electronic properties of both $LiCoO_2$ modifications are tunable through delithiation while the basic structural frameworks are maintained. This provides a unique opportunity to assign the respective influence of structures and electronic properties on the water oxidation properties. While spinel-type $LiCoO_2$ with $\{Co_4O_4\}$ cubane motifs is active for photochemical water oxidation, the layered modification without cuboidal structural elements is nearly inactive. Here, we demonstrate that the water oxidation performance of both modifications can be significantly improved through chemical delithiation. A wide range of analytical methods were applied to investigate the transition of electronic properties upon delithiation, and a direct correlation between enhanced hole mobility and improved water oxidation activity was established. The difference in water oxidation activities between the two structural modifications was further linked to the role of $\{Co_4O_4\}$ cubane motifs in constructing 3D Co−O−Co networks with expanded hole transfer paths. Thus, the promoting effects of both delithiation and $\{Co_4O_4\}$ cubane motifs on water oxidation can be consistently explained by enhanced hole mobility.

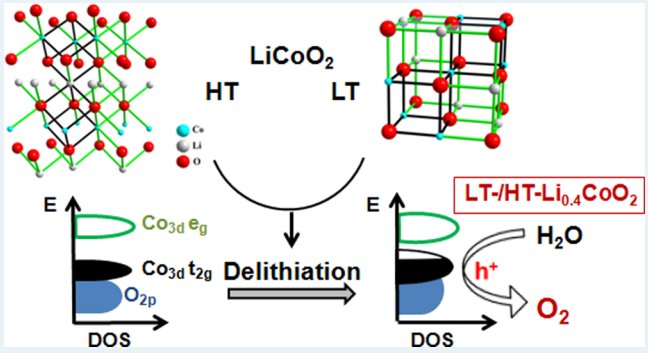

KEYWORDS: *photocatalysts, water oxidation, oxygen evolution, lithium cobalt oxides, electronic properties, hole mobility, delithiation*

INTRODUCTION

Conversion of solar energy into chemical fuels by artificial photosynthesis could provide a sustainable and flexible solution to current energy and climate problems.[1] To date, one of the most demanding steps toward solar water splitting remains the development of efficient and economic water oxidation catalysts (WOCs).[2] Even after decades of synthetic and mechanistic studies, the complex multistep processes of water oxidation with heterogeneous catalysts are not completely understood.[3] Mechanistic insight requires highly sophisticated in situ techniques which are currently being developed.[4]

In a search for general WOC design concepts, cuboidal $\{M_4O_4\}$ motifs (M = Co, Mn) inspired by the $\{CaMn_4O_5\}$ oxygen evolving cluster (OEC) in photosystem II[5] have been established as an effective design paradigm[6] for molecular-,[7] oxide-,[8] and polyoxometalate-based[9] WOCs. Nevertheless, the precise impact of $\{M_4O_4\}$ cubane motifs on the oxygen evolution performance remains a topic of extensive debate,[10] with the amorphous Co-Pi electrocatalysts[11] as a typical example. The absence of long-range order renders structure−activity relations of amorphous Co-Pi type WOCs rather difficult to clarify,[12] so that the precise mechanistic role of the proposed $\{Co_4O_4\}$ building blocks remains under investigation.[13]

While many water oxidation active oxides, such as Co_3O_4, $LiCoO_2$, and λ-MnO_2,[8a,b] share $\{M_4O_4\}$ as a common construction motif, other oxide-based materials without cubane units (e.g., $Co(OH)_2$ and Co-Fe hydroxides and oxyhydroxides) are capable of oxidizing water as well.[14] Moreover, a very recent study ascribed the water oxidation activity of the widely investigated $\{Co^{III}_4O_4\}$-based $Co_4O_4(OAc)_4(py)_4$ molecular WOC to Co^{2+} impurities instead of the proposed active $\{Co_4O_4\}$ cubane moieties.[15] This calls for further investigations on structure−activity correlations.

Received: January 15, 2015
Revised: May 13, 2015
Published: May 13, 2015

DOI: 10.1021/acscatal.5b00078
ACS Catal. 2015, 5, 3791−3800

$LiCoO_2$ has been widely applied and investigated as a battery material, whereas its full potential for photocatalytic water oxidation is just beginning to be explored.[8b] Recently, the structural differences between layered $LiCoO_2$ (high-temperature modification, HT-$LiCoO_2$) and spinel $LiCoO_2$ (low-temperature modification, LT-$LiCoO_2$) were linked to their different properties as cathode materials and WOCs, respectively. The layered arrangement of $\{CoO_6\}$ units in HT-$LiCoO_2$ allows for reversible Li^+ extraction−reintercalation and electronic structure transformations without changing the basic 2D structural framework. LT-$LiCoO_2$ is based on the same oxygen sublattice, albeit with mixed Co/Li (0.25/0.75 and vice versa) occupancies on alternating {111} planes, resulting in $\{Co_4O_4\}$ motifs (marked in yellow in Figure 1) related to the

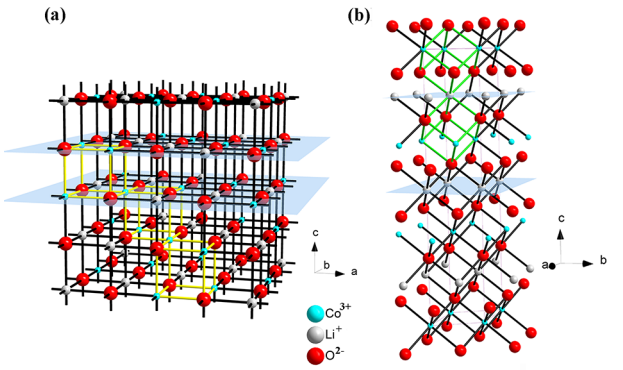

Figure 1. Structural models of (a) spinel-type LT-$LiCoO_2$ (yellow pattern; 3D Co−O−Co network composed of $\{Co_4O_4\}$ cubane motifs) and (b) layered HT-$LiCoO_2$ (green pattern; 2D Co−O−Co layers separated by Li^+).

cuboidal OEC in photosystem II. While the battery material HT-$LiCoO_2$ is nearly inactive for water oxidation, the electrochemically less relevant LT form displays considerably higher water oxidation activity, which was assigned to its catalytically active $\{Co_4O_4\}$ moieties.[8b]

Most recently, the influence of delithiation on the electrochemical water oxidation activity of $LiCoO_2$ oxides was investigated in two parallel studies.[16] However, different conclusions were reached in these works. Whereas one study emphasized the beneficial role of delithiation for oxygen evolution, the second investigation indicated that it was detrimental to water oxidation. A further related study[17] even revealed the formation of amorphous layers or phase transitions on the surface of $LiCoO_2$ together with in situ delithiation during electrochemical water oxidation, which renders the overall assessment of the water oxidation activity of this material even more complex.

Therefore, the precise impact of delithiation on the water oxidation activity of $LiCoO_2$ materials needs to be further clarified. In the following, we newly investigate photochemical water oxidation with pristine and chemically delithiated $LiCoO_2$ modifications in detail. The standard $[Ru(bpy)_3]Cl_2/Na_2S_2O_8$ protocol was selected to evaluate the water oxidation activity of $LiCoO_2$, because it was reported to leave the surface structure of WOCs intact during water oxidation.[18] A wide range of analytical techniques (including FT-IR, UV/vis, Raman, ^{7}Li NMR, and XPS spectroscopy and magnetic susceptibility measurements) was applied to assess the impact of delithiation and $\{Co_4O_4\}$ moieties on the water oxidation performance. The tolerance of both LT and HT structural frameworks to delithiation allowed us to differentiate between the influences of structural and electronic properties on water oxidation. A direct correlation among structure, electronic properties, and water oxidation activity was successfully established. Bioinspired architectures ($\{Co_4O_4\}$ moieties) and tuning of the electronic properties via delithiation both work in the same direction toward optimization of charge carrier transport properties for improved water oxidation performance (Scheme 1).

Scheme 1. Optimization Strategies for Photochemical Water Oxidation with $LiCoO_2$ Modifications by Targeting Their Electronic Properties

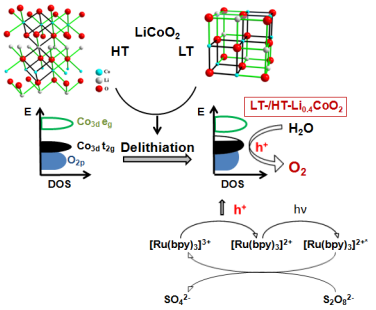

RESULTS AND DISCUSSION

Synthesis and Structure. Samples of LT- and HT-$LiCoO_2$ were synthesized via a standard citrate sol−gel route.[19] TG-DSC analyses (Figure S1 in the Supporting Information) indicate the onset of LT-$LiCoO_2$ formation around 400 °C, followed by an exothermic phase transition to HT-$LiCoO_2$ in the range of 550−800 °C with no further weight loss. Transformation of LT- into HT-$LiCoO_2$ is evident from the appearance of the additional (006) and (018) peaks (Figure 2)

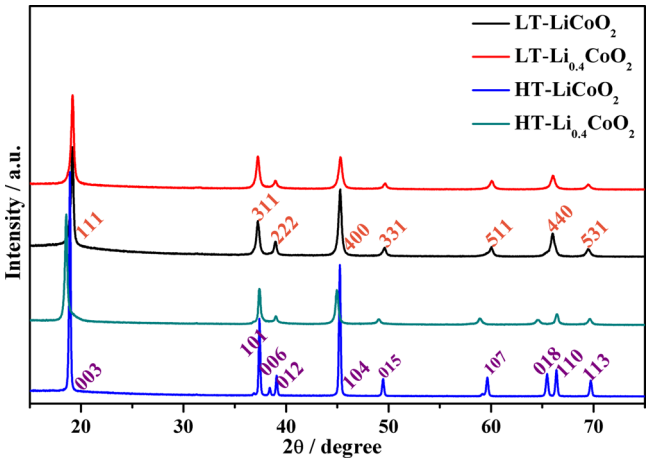

Figure 2. PXRD patterns of $LiCoO_2$ samples before and after delithiation.

in the powder X-ray diffraction (PXRD) patterns.[19] Raman spectroscopy (Figure S2 in the Supporting Information) permits a better differentiation between spinel-type LT-$LiCoO_2$ ($Fd3m$, four active bands around 605, 590, 484, and 449 cm^{-1}) and the layered HT form ($R\bar{3}m$, two active bands at 597 and 487 cm^{-1}).[20]

DOI: 10.1021/acscatal.5b00078
ACS Catal. 2015, 5, 3791−3800

Both fully lithiated starting materials were converted into LT-/HT-$Li_{0.4}CoO_2$, respectively, through chemical delithiation in a bromine−acetonitrile solution. Regardless of the applied treatment time (7 days was selected as the standard procedure for all WOCs discussed below), the degree of delithiation remained constant around $Li_{0.4}CoO_2$ for HT and LT phases (Table S6 in the Supporting Information), which is in line with the reported lithium content of 0.49 with bromine as oxidant and the degree of delithiation as a function of oxidation potential.[21]

Both HT- and LT-$Li_{0.4}CoO_2$ maintained their basic structural motifs after delithiation while exhibiting the expected lattice constant changes.[22] LT-$Li_{0.4}CoO_2$ undergoes contraction along *b* and *c*, whereas HT-$Li_{0.4}CoO_2$ displays shortened *a* and *b* axes along with an expansion along the *c* axis due to decreasing electrostatic attraction between the $\{CoO_6\}$ layers (Table S1 in the Supporting Information). The slightly asymmetric peak profile of HT-$Li_{0.4}CoO_2$, in particular of the (003) reflection (Figure S45 in the Supporting Information), may indicate the onset of sliding of the oxygen layers as observed for deeper delithiated Li_xCoO_2 phases ($x < 0.35$).[23] The HT form underwent peak broadening during delithiation which is ascribed to an increase in lattice strain, given that particle sizes and BET surface areas remain within the same order of magnitude for both modifications (Figures S3 and S4 and Table S1 in the Supporting Information).

Photochemical Water Oxidation Performance. The photochemical water oxidation activity of pristine and delithiated LT/HT-$LiCoO_2$ was evaluated according to a standard protocol with $[Ru(bpy)_3]^{2+}$ as photosensitizer and $S_2O_8^{2-}$ as sacrificial electron acceptor. A 470 nm LED with an intensity of 5000 lux was used as the light source. Oxygen evolution was monitored by gas chromatography (GC) of the head space and by Clark electrode techniques in solution, respectively. In order to record the WOC activities of the four title compounds under standardized conditions for the sake of comparability, the test conditions (e.g., pH, light intensity, buffer, stirring speed, and degassing and ultrasonic dispersing times) for photocatalytic measurements were selected and fixed according to our previous studies.

In line with previous reports,[8b] both Clark electrode (Figure 3) and GC based (Figure 4) results consistently indicate that spinel-type LT-$LiCoO_2$ is more active than layered HT-$LiCoO_2$, which produces only low quantities of oxygen.

Most importantly, the water oxidation activities of both compounds were notably enhanced after delithiation: LT-$Li_{0.4}CoO_2$ and HT-$Li_{0.4}CoO_2$ display 5- and 10-fold higher oxygen evolution in solution under equilibrium conditions (525 and 250 μmol/L, respectively; cf. Figure 3) in comparison to the pristine spinel and layered oxides. Commercial Co_3O_4 nanoparticles were also investigated under the same conditions as the reference sample. LT-$Li_{0.4}CoO_2$ produced an even slightly higher oxygen concentration after equilibrium was reached (Figure S9 in the Supporting Information). As numerous previous studies revealed the significant influence of BET surface area on the water oxidation performance,[24] GC-based activities were furthermore normalized to BET surfaces. As shown in Figure 4, the productive effect of delithiation on the water oxidation activity remains significant after normalization: LT (2.1 μmol m^{-2} raised to 10.9 μmol m^{-2}) and HT (1.0 μmol m^{-2} raised to 9.8 μmol m^{-2}). Therefore, the remarkably enhanced water oxidation performance of both modifications cannot be solely explained by surface effects.

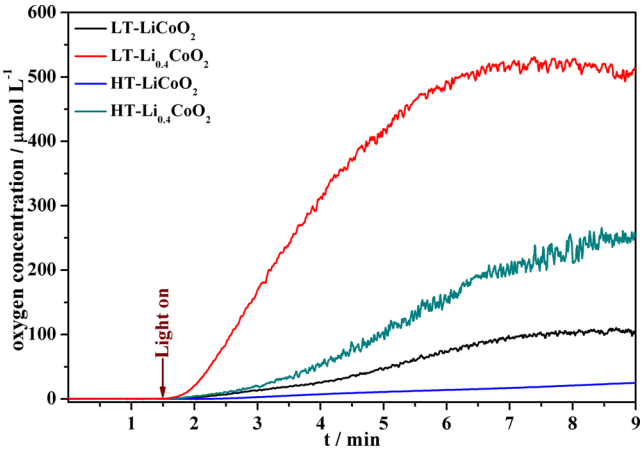

Figure 3. Oxygen evolution in solution for $LiCoO_2$ samples before and after delithiation (Clark electrode monitoring in solution; 10 mg of WOC, 1.33 mM $[Ru(bpy)_3]Cl_2$, 26.25 mM $Na_2S_2O_8$, 8 mL of pH 7 phosphate buffer in 0.1 M, 470 nm LED (5000 lux intensity)).

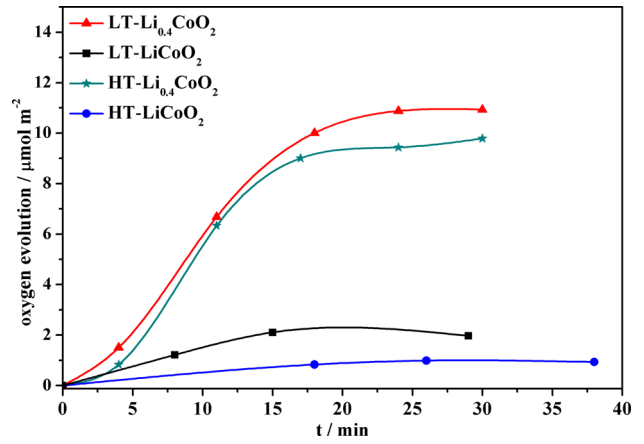

Figure 4. Oxygen evolution in solution for $LiCoO_2$ samples before and after delithiation normalized to BET surface area (GC detection in headspace; 10 mg of WOC, 1.33 mM $[Ru(bpy)_3]Cl_2$, 26.25 mM $Na_2S_2O_8$, 8 mL of pH 7 phosphate buffer, 470 nm LED (5000 lux intensity)).

These results are in line with our recent study on Co_3O_4, which indicates that surface area is not necessarily the most influential factor in water oxidation.[25] TOF values based on BET surface and oxygen evolution rate were compared to those of Co_3O_4 WOCs reported in our previous study (Table S1 in the Supporting Information). The maximum TOF value of 9×10^{-3} μmol s^{-1} m^{-2} for LT-$Li_{0.4}CoO_2$ is 2.5 times higher than the TOF for nanocrystalline Co_3O_4 under identical measurement conditions.[24]

Cyclic voltammetry was furthermore conducted to investigate electrochemical water oxidation with the four title lithium cobalt oxide compounds (Figure S39 in the Supporting Information). In line with the photochemical results, the delithiated LT/HT-$Li_{0.4}CoO_2$ materials displayed higher activities than their pristine LT/HT-$LiCoO_2$ counterparts. However, the productive effect of delithiation on the electrochemical water oxidation performance is not as significant as that on the photochemical process. These observations agree well with recent studies on cobalt iron oxides.[18]

DOI: 10.1021/acscatal.5b00078
ACS Catal. 2015, 5, 3791−3800

Generally, the electrochemical process differs considerably from photochemical conditions with respect to the accumulation of much higher charge densities on the electrode surfaces which leads to higher quantities of evolved oxygen. This is likely to exert a much more drastic impact on the catalyst properties than milder photochemical conditions. As for recent progress on cobalt iron oxide catalysts,[18] HRTEM investigations indeed revealed the formation of an amorphous layer on the particle surface after electrochemical water oxidation, while their surface was retained during the photochemical process. The stronger influence of electrochemical water oxidation on the nature of the catalyst in comparison to photochemical protocols has also been reported for prominent polynuclear cluster WOCs. Recent works, for example, indicate that $[Co_4(H_2O)_2(\alpha\text{-}PW_9O_{34})_2]^{10-}$ operates as a homogeneous catalyst under photochemical conditions, while it is transformed into heterogeneous CoO_x catalysts in electrochemical setups.[26]

The essential catalytic role of delithiated LT-/HT-$Li_{0.4}CoO_2$ WOCs was verified by excluding Co^{2+} leaching as a significant contribution to of total water oxidation activity. As shown in Figure S11 in the Supporting Information, nearly 1000-fold higher Co^{2+} concentration in comparison to that for the leached Co^{2+} from lithium cobalt oxides (Table S2 in the Supporting Information) is required to obtain oxygen evolution comparable to that of LT-$Li_{0.4}CoO_2$. Major structural changes during water oxidation were excluded through comparison of PXRD patterns of LT-$Li_{0.4}CoO_2$ before and after water oxidation (Figure S17 in the Supporting Information). Co 2p, Co 3p, and valence band spectra further confirm that LT-$Li_{0.4}CoO_2$ underwent no significant surface changes (Figure S18 in the Supporting Information) during photochemical water oxidation. UV/vis (Figure S19 in the Supporting Information) and FT-IR spectra (Figure S20 in the Supporting Information) of LT-$Li_{0.4}CoO_2$ indicate that the metallic properties (discussed below) were retained after water oxidation. In contrast, PXRD patterns of HT-$Li_{0.4}CoO_2$ displayed a broadening of the (003) reflection (Figure S22 in the Supporting Information) after water oxidation, which points to an adjustment of the interlayer distance, probably through uptake of water or other species. The morphology of LT-$Li_{0.4}CoO_2$ before and after water oxidation was examined by HR-TEM (Figure 5). Other than in electrochemical studies,[16,27] no amorphous layers were present on the edge of the particles after photochemical water oxidation. The lattice distances determined from HR-TEM images correspond well to the PXRD patterns, thereby excluding phase transitions after water oxidation. ^{18}O labeling experiments identify water as the exclusive oxygen source, because the ratios among $^{16}O^{16}O$, $^{16}O^{18}O$, and $^{18}O^{18}O$ fit well with theoretical values for the experimentally used 10% ^{18}O containing water (Figures S54–S57 in the Supporting Information).

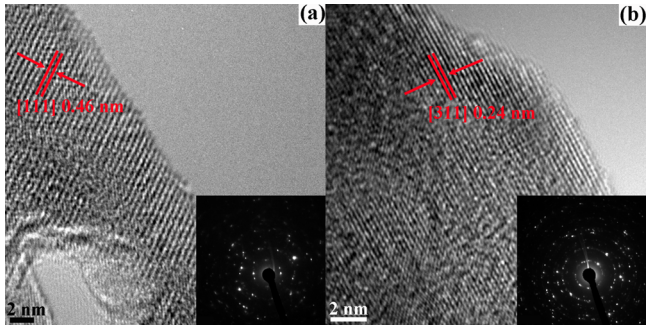

Figure 5. HR-TEM pictures of LT-$Li_{0.4}CoO_2$ before (a) and after (b) water oxidation (inset: SAED patterns, scale bar 2 nm).

A previous study indicated that LT-$LiCoO_2$ is stable under photochemical conditions after a single water oxidation run.[8b] Here, we further investigated the long-term stability of all catalysts through five continuous water oxidation runs. Interestingly, the recovered LT-$LiCoO_2$, LT-$Li_{0.4}CoO_2$, and HT-$LiCoO_2$ even displayed increased water oxidation activity in the second run (Table S3 in the Supporting Information). ICP-AES analyses of the supernatant solutions after the first run revealed minor lithium leaching (Table S2 in the Supporting Information), which explains their improved water oxidation activity. In contrast, recovered HT-$Li_{0.4}CoO_2$ shows only ca. 50% catalytic activity in the second run (Figure S24 in the Supporting Information), which is probably due to the aforementioned structural adjustment ((003) peak broadening of PXRD pattern, Figure S22 in the Supporting Information) after the first water oxidation cycle that outweighs the influence of delithiation. Further water oxidation runs led to decreased activity of all four WOCs (Figures S25–S27 and Table S3 in the Supporting Information). Nevertheless, LT-$Li_{0.4}CoO_2$ still displays the highest performance after five cycles. HR-TEM pictures (Figure S28 in the Supporting Information) of LT-$Li_{0.4}CoO_2$ confirm the absence of amorphous layers even after the fifth run. PXRD (Figures S29–S32 in the Supporting Information) and SAED patterns (Figure S28) as well as EXAFS spectra (Figure S35 in the Supporting Information) ensured that the structure frameworks of the catalysts were retained after photochemical water oxidation. However, the observed significant reflection broadening of the PXRD patterns (Figures S31 and S32) implies decreasing crystallinity, which might be associated with an increase of lattice defects due to cobalt leaching (Table S2). These factors may explain the decrease in water oxidation activity after the second run. Furthermore, samples subjected to shorter delithiation periods of 1–2 h ($Li_{0.84}CoO_2$ and $Li_{0.63}CoO_2$) display lower O_2 evolution activity than the title compounds (Figure S52 in the Supporting Information).

In summary, delithiation significantly improved the water oxidation performance for both $LiCoO_2$ modifications, especially for HT-$LiCoO_2$, which underwent a transition from a nearly inactive material to an active water oxidation catalyst. Not only is this profound influence exerted on photochemical water oxidation but it is also evident from a significant transformation of the electronic structure. In the following, we investigate the influence of delithiation on the electronic properties in detail.

Electronic Properties. Regardless of their structural differences, both LT-$LiCoO_2$ and HT-$LiCoO_2$ display similar absorption properties in the visible light range with broad absorption edges around 700–750 nm. They are transformed into strong absorption bands extending beyond 850 nm (Figure 6 and Figure S47 in the Supporting Information) upon delithiation, implying significantly decreased band gaps (consistently determined from Tauc plots for $LiCoO_2$ as either direct or indirect semiconductor, cf. Figure S36 in the Supporting Information). Furthermore, the disappearance of all characteristic FT-IR bands (Co–O and Li–O vibration modes) below ca. 600 cm^{-1} for LT-/HT-$Li_{0.4}CoO_2$ (Figure 7 and Figure S46 in the Supporting Information) along with the remarkably low transmission in the 700–1000 cm^{-1} range

DOI: 10.1021/acscatal.5b00078
ACS Catal. 2015, 5, 3791–3800

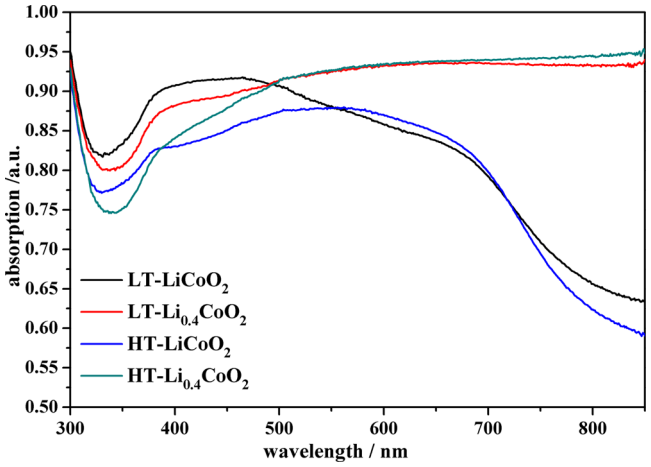

Figure 6. UV/vis spectra of LT-$LiCoO_2$, HT-$LiCoO_2$, LT-$Li_{0.4}CoO_2$, and HT-$Li_{0.4}CoO_2$.

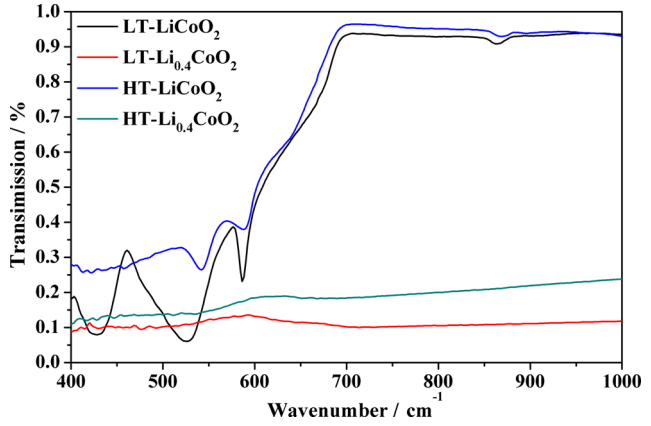

Figure 7. FT-IR spectra of LT-/HT-$LiCoO_2$ and LT-/HT-$Li_{0.4}CoO_2$.

points to strong IR reflection by free electrons and to an emerging metallic character.[23] The formation of highly mobile holes in the Co 3d t_{2g} band upon delithiation is likely to reduce the characteristic wavelength-dependent absorption through oscillation to any incident frequency. Electrochemical impedance studies (Figure S38 in the Supporting Information) revealed a remarkable resistance decrease after delithiation, which further verifies the insulator (or semiconductor) to metal transition.

Magnetic susceptibility measurements in combination with ^{7}Li NMR spectroscopy provided deeper insight into the positive effect of enhanced charge carrier mobility on the water oxidation activity of LT- and HT-$Li_{0.4}CoO_2$. The temperature-dependent magnetic susceptibilities of pristine and delithiated lithium cobalt oxides were recorded in both heating and cooling modes over the temperature range 5−300 K (Figure 8 has a minor hysteresis loop due to residual oxygen after evacuation (Figure S37 in the Supporting Information)).[28] All samples exhibited paramagnetic behavior above 100 K, and straightforward Curie−Weiss fits afford Curie constants (in emu K Oe^{-1} mol^{-1}) and effective magnetic moments (μ_{eff}, equal to charge carriers per cobalt atom) of 0.095 (0.33 μ_B) for both LT- and HT-$LiCoO_2$, in comparison to 0.315 (0.88 μ_B) and 0.236 (0.70 μ_B) for LT- and HT-$Li_{0.4}CoO_2$, respectively (cf. inset in Figure 8).

^{7}Li magic-angle-spinning (MAS) NMR spectra for LT-/HT-$LiCoO_2$ display the expected main peaks at 0 ppm for Li^+ in a

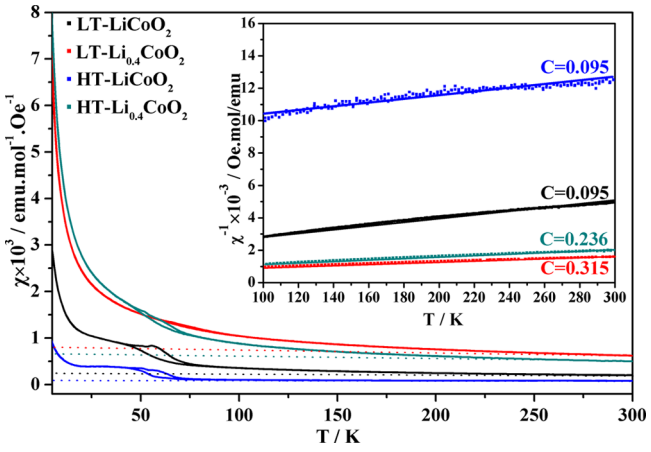

Figure 8. Temperature-dependent magnetic susceptibility of LT-/HT-$LiCoO_2$ and LT-/HT-$Li_{0.4}CoO_2$ in the 5−300 K range.

diamagnetic environment of LS Co^{3+} centers with symmetrically positioned sidebands (Figure 9).[28] Delithiation induces a

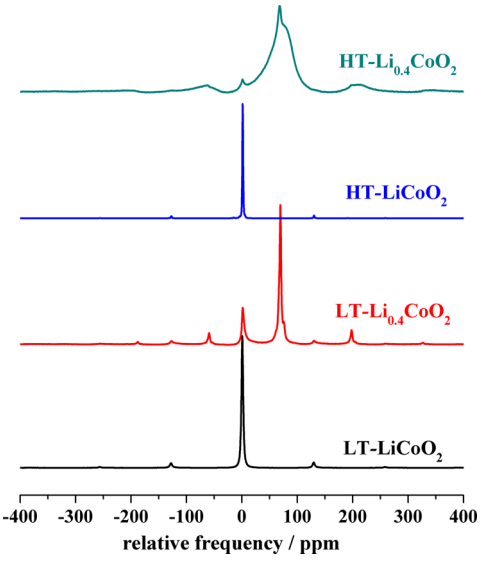

Figure 9. ^{7}Li NMR MAS spectra of LT-/HT-$LiCoO_2$ and LT-/HT-$Li_{0.4}CoO_2$.

split of the main peak into two peaks located at ca. 0 and 70 ppm for both LT- and HT-$Li_{0.4}CoO_2$, indicating the presence of two different lithium sites surrounded by diamagnetic and paramagnetic centers, respectively. The most intense peak underwent a Knight shift to ca. 70 ppm arising from the presence of free electrons, thus providing evidence for the delocalization of t_{2g} holes,[28] in line with the temperature-independent susceptibility data. HT-$Li_{0.4}CoO_2$ displays a considerable line broadening in comparison to the delithiated LT-spinel type, which corresponds well to the presence of a shoulder for the (003) reflection after delithiation (PXRD pattern, Figure 2), pointing to a higher degree of disorder in the packing of the Co−O layers (*ab* planes in Figure 1) upon delithiation as well as intense lattice strains.

The oxidative effect of chemical delithiation is evident from the characteristic Co $2p_{3/2}$ and Co $2p_{1/2}$ XPS peaks located around 779 and 795 eV, respectively, as well as from their MLCT satellites at ca. 10 eV higher binding energies (Figure 10).[29] The broadening of the Co 2p peaks toward higher

DOI: 10.1021/acscatal.5b00078
ACS Catal. 2015, 5, 3791−3800

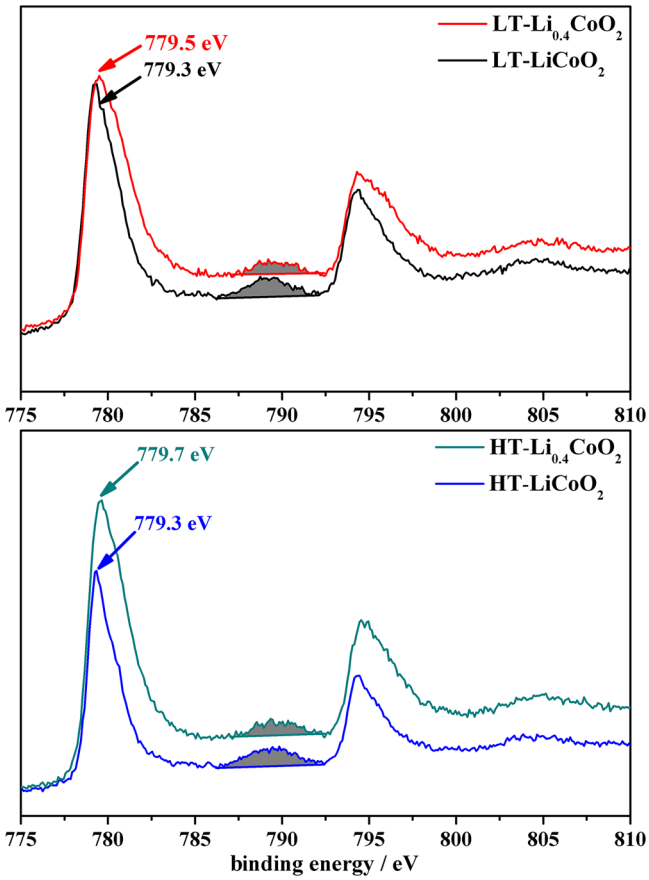

Figure 10. Co 2p XPS spectra of LT-/HT-$LiCoO_2$ and LT-/HT-$Li_{0.4}CoO_2$.

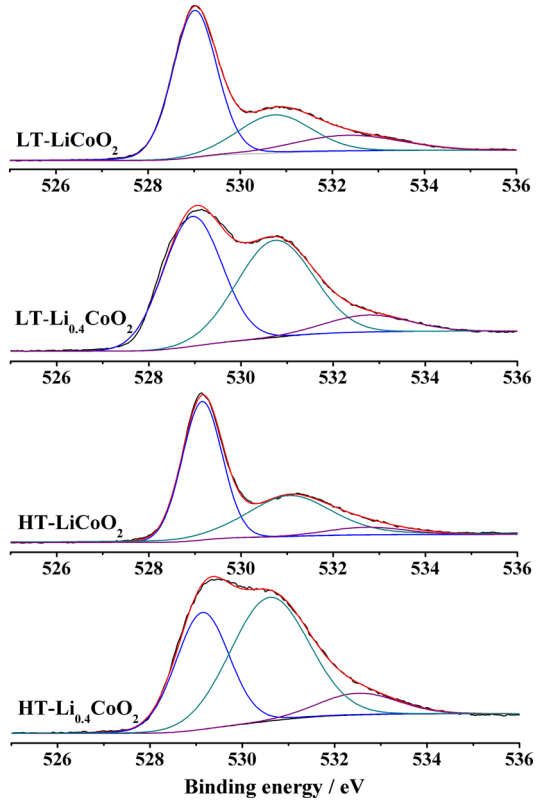

Figure 11. O 1s XPS spectra of LT-/HT-$LiCoO_2$ and LT-/HT-$Li_{0.4}CoO_2$.

binding energy and decreasing areas of the satellite peaks around 789 eV (gray areas in Figure 10) confirm the presence of Co^{4+} in LT-/HT-$Li_{0.4}CoO_2$. O 1s XPS spectra of all compounds (Figure 11) are constituted of three components around 529, 531, and 533 eV, respectively. Whereas the highest and lowest energy peaks can be well ascribed to surface absorbed oxygen molecular and lattice oxygen species, respectively, the assignment of the peak around 531 eV, which displays lower intensity after delithiation, is less straightforward and was the source of controversy in previous studies.

The decreased fraction of lattice oxygen species at around 529 eV and an increased contribution from the middle peak most likely point to the partial oxidation of O^{2-} ions for overall charge compensation via Co t_{2g} hole delocalization after delithiation, resulting in stronger covalence of Co−O bonds and increased binding energy of lattice oxygen.[30] This hypothesis is further supported by the stronger dispersion and overlap of the Co 3d−minor Co 2p (0−2 eV) and O 2p (3−8 eV) valence band (Figure 12) as well as by the observed decrease in Co−O bond lengths (Table 1) after delithiation. Moreover, the onset shift of the valence band edges toward lower bond energies (i.e., closer to the e_g conduction band) for LT-/HT-$Li_{0.4}CoO_2$ is well in line with the band gap narrowing determined from UV/vis spectra (Figure S36 in the Supporting Information).

Correlation among Structure, Electronic Properties, and Water Oxidation Activity. The corresponding effects of delithiation on water oxidation activity as well as on a wide range of spectroscopic characteristics imply a strong correlation between catalytic performance and electronic properties. Both temperature-independent susceptibility and photochemical water oxidation activity display the same trend: LT-$Li_{0.4}CoO_2$ > HT-$Li_{0.4}CoO_2$ > LT-$LiCoO_2$ > HT-$LiCoO_2$. This suggests that itinerant charges, especially the mobile holes involved in water oxidation, could be the major driving force for the activity improvement. Enhanced hole mobility after delithiation is furthermore evident from multiple characterizations: (a) pronounced metallic character (cf. UV/vis, FT-IR, and ^{7}Li NMR spectra), (b) formation of Co^{4+} centers which give rise to higher hole concentrations in the valence band (reflected in higher magnetic moments), and (c) enhanced hybridization of Co 3d and O 2p bands (cf. valence band and O 1s XPS spectra), resulting in improved Co 3d t_{2g} hole mobility. The electronic property transition upon delithiation was further complemented with DFT calculations (Figures S40 and S41 in the Supporting Information).

The remarkably higher carrier mobility is furthermore illustrated by a sharp decrease of ac resistance upon delithiation (from 7 to 0.04 kΩ for LT forms and from 700 to 30 kΩ for HT forms; Table 1). Due to the anisotropic conductivity of the HT structure, polycrystalline-based measurements lead to significantly overestimated resistance for HT-$LiCoO_2$ and HT-$Li_{0.4}CoO_2$. A more balanced comparison between LT and HT forms would require anisotropic conductivity measurements on single-crystal samples.[31]

The conductivity properties (anisotropic or isotropic) of the two $LiCoO_2$ modifications can be directly correlated to the presence or absence of $\{Co_4O_4\}$ units. As the conductivity arises from electron transport through a Co 3d−O 2p covalent interaction, the presence of $\{Co_4O_4\}$ in LT-$LiCoO_2$ and LT-

DOI: 10.1021/acscatal.5b00078
ACS Catal. 2015, 5, 3791−3800

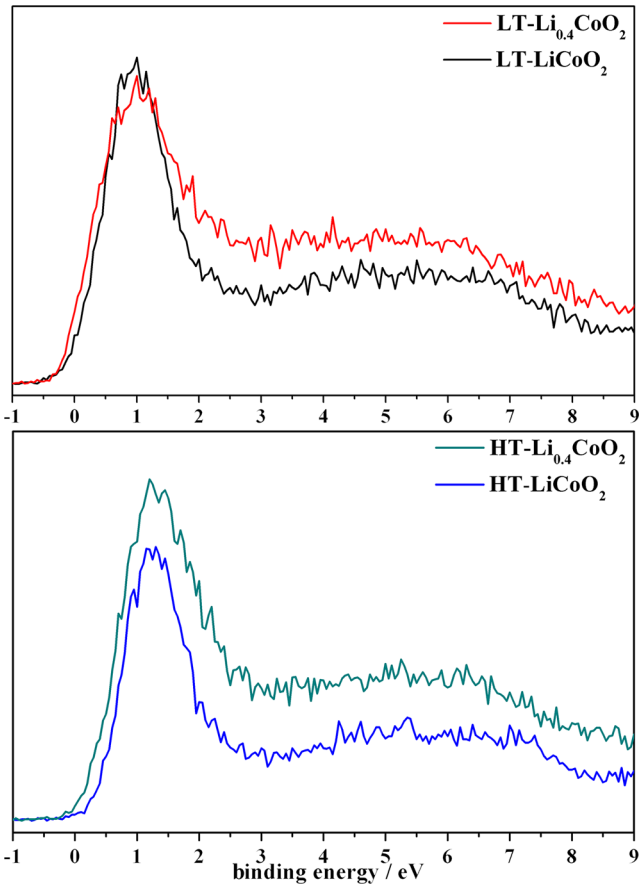

Figure 12. Valence band spectra of LT-/HT-$LiCoO_2$ and LT-/HT-$Li_{0.4}CoO_2$.

$Li_{0.4}CoO_2$ extends the Co−O−Co bonds into a 3D network (yellow traces in Figure 1) and facilitates hole transfer in all directions, while the absence of $\{Co_4O_4\}$ units in HT-$LiCoO_2$ and HT-$Li_{0.4}CoO_2$ limits the hole transfer in a single 2D Co−O−Co layer (*ab* planes in Figure 1). This explains the higher water oxidation activity (before normalization) for LT-$LiCoO_2$ and LT-$Li_{0.4}CoO_2$ in comparison to HT-$LiCoO_2$ and HT-$Li_{0.4}CoO_2$, respectively. Analogously, a very recent study on $LiCoO_2$ for electrochemical water oxidation and oxygen reduction also revealed the impact of charge transfer processes on the catalytic activity.[16b,32]

The water oxidation activity of various catalyst types, such as perovskites and lithium battery materials, was generally perceived to be strongly influenced by their surface states. However, recent studies also showed that the activities of two representative materials may still be different, regardless of the formation of virtually identical Co-Pi layers on their surface under electrochemical water oxidation conditions. Consequently, the overall water oxidation performance was not solely determined by such Co-Pi layers but also partially arose from the bulk substrate.[17] Furthermore, a recent investigation of perovskite materials for electrochemical water oxidation revealed the influence of substrates and of bulk conductivity on water oxidation as well.[33]

The mechanisms of O−O bond formation are currently the focus of manifold studies,[34] while less emphasis has been placed on relationships between electronic properties and dye-sensitized charge transfer processes. The complex and heterogeneous hole scavenging steps between oxide WOCs and $[Ru(bpy)_3]^{3+}$ (cf. Scheme 1) are currently under mechanistic and kinetic investigation.[35] As four hole transport steps are required for the formation of an O_2 molecule, the efficiency of hole transfer across the WOC and the heterogeneous interface is very likely to be a crucial step. Acceleration of water oxidation kinetics by WOCs with increased Co−O bond covalence was ascribed to a stronger affinity between cobalt sites and surface absorbed oxygen species (such as hydroxyl groups).[16b] However, further investigations are necessary to determine whether this increased affinity also facilitates the interface hole transfer between WOCs and incoming oxygen species.

The present results demonstrate that the absence of a 3D conducting network in HT-$LiCoO_2$ can be overcompensated through delithiation with significantly enhanced covalent character of Co−O bonds. The major correlations among structure, electronic properties, and water oxidation activity can be summarized as follows, (1) Delithiation of both $LiCoO_2$ modifications leads to increased hole concentration together with more covalent and shorter Co−O bonds. (2) The presence of $\{Co_4O_4\}$ motifs expands Co−O−Co pathways into a 3D charge carrier transportation network with isotropic conductivity. (3) Chemical delithiation further strengthens the role of $\{Co_4O_4\}$ motifs. (4) The improvement in water oxidation activity caused by both delithiation and $\{Co_4O_4\}$ motifs can be consistently explained by enhanced hole mobility. The role of hole mobility was further confirmed by our current study on related material systems whose photochemical water oxidation activities can be flexibly tailored by their tunable electronic properties.

CONCLUSIONS

The HT and LT forms of $LiCoO_2$ featuring 3D biomimetic $\{Co_4O_4\}$ cubane motifs and 2D layer structures, respectively, were selected as models to study the correlation among structure, electronic properties, and dye-sensitized photo-

Table 1. Correlation among Structure, Delithiation, Electronic Properties, and Water Oxidation Performance of Fully Lithiated and Delithiated $LiCoO_2$ WOCs

WOC	Co−O network/ $\{Co_4O_4\}$	Co−O distance (Å)	Co−O hybridization	μ_B	X_c[a] (emu mol^{-1} Oe^{-1})	resistance (kΩ (ac))	resistivity[31] (Ω cm^{-1})	O_2(abs) (μmol)	O_2(BET)[b] (μmol m^{-2})
LT-$LiCoO_2$	3D/yes	1.9271(12)	weak	0.33	0.200	7		0.48	2.1
LT-$Li_{0.4}CoO_2$	3D/yes	1.8934(17)	strong	0.88	0.625	0.04		4.57	10.9
HT-$LiCoO_2$	2D/no	1.9159(7)	weak	0.33	0.084	700	5 (*ab* plane), 4000 (⊥ *ab* plane)	0.15	1.0
HT-$Li_{0.4}CoO_2$	2D/no	1.8697(17)	strong	0.70	0.514	30	0.009 (*ab* plane of $Li_{0.5}CoO_2$)	1.79	9.8

[a] X_c = temperature-independent susceptibility. [b] Normalized to absolute surface area (BET × sample mass).

DOI: 10.1021/acscatal.5b00078
ACS Catal. 2015, 5, 3791−3800

catalytic water oxidation. Chemical delithiation of both forms results in significantly improved water oxidation activity in comparison to the fully lithiated parent compounds. This performance enhancement goes hand in hand with a significant transition of the electronic properties toward metallic behavior upon delithiation. Characterization of the electronic structure with a wide spectrum of analytical techniques indicates that hole mobility is most likely to be the major driving force behind the enhanced water oxidation activity. Cuboidal $\{Co_4O_4\}$ motifs were identified as the basic building blocks of 3D Co−O−Co charge transport networks for enhanced hole transfer efficiency. Their networking role is further reinforced through stronger covalent character of the Co−O bonds after delithiation. These results pave the way to new optimization strategies for water oxidation catalysts through combined control over structural and electronic properties.

EXPERIMENTAL SECTION

Synthetic Methods. $LiCoO_2$ nanoparticles were synthesized via a conventional sol−gel method as follows: 10 mmol of Li_2CO_3, 20 mmol of $Co(NO_3)_2{\cdot}6H_2O$, 40 mmol of citric acid, and 60 mmol of urea were dissolved in 300 mL of deionized water. The as-prepared solution was stirred and condensed at 80 °C into a gel which was further decomposed at 170 °C over 4 h into a foamlike precursor. Both LT-$LiCoO_2$ and HT-$LiCoO_2$ were obtained from calcination of the above precursor at 400 and 700 °C for 5 h, respectively. Lithium extraction of as-synthesized LT-$LiCoO_2$ and HT-$LiCoO_2$ in a bromine−acetonitrile solution (4 mL of Br_2 and 10 mL of acetonitrile) for 7 days afforded LT- and HT-$Li_{0.4}CoO_2$ as products.

Photocatalytic Tests. WOC tests were performed according to well-established $[Ru(bpy)_3]^{2+}/S_2O_8^{2-}$ protocols. First, a suspension was prepared by mixing 10 mg of water oxidation catalyst, 8 mg of $[Ru(bpy)_3]Cl_2$ photosensitizer, and 50 mg of $Na_2S_2O_8$ in 8 mL of KPi buffer (0.1 M, pH 7, 10 mL vial) in a dark cabinet. Next, the suspension was degassed with helium to remove O_2 in both the solution and the head vial. An LED lamp with 470 nm wavelength and 5000 lux output was used as the visible light source. Oxygen production was monitored with a calibrated Clark electrode (Unisense, stirring sensitivity <2%, response time (90%) <10 s) online in solution or by gas chromatography (Agilent 7820A packed with a 3 m × 2 mm molecular sieve 13X 80-100 column). A 100 μL portion of gas from the headspace was injected into a gas chromatograph using a gastight microliter syringe (Hamilton 1825 RN) over intervals of several minutes. Helium was chosen as carrier gas to increase the detection sensitivity of O_2 relative to N_2. Gases were detected with a thermal conductivity detector (Varian) operated at 200 °C. Contamination of the headspace by air was constantly monitored through the N_2 peak on GC chromatograms. Calibration was performed by injection of known quantities of pure oxygen diluted in an equivalent vial containing the same volume and concentration of buffered solution used for the measurements.

Analytical Techniques. Powder X-ray diffraction patterns (PXRD patterns) were recorded on a XPERT-PRO diffractometer (reflection mode, step size 0.04°/step, 15 s/step) with Cu $K_{\alpha1}$ radiation or on a STOE STADI P diffractometer (transmission mode, step size 2.09°/step, 35 s/step) with Co $K_{\alpha1}$ or Cu $K_{\alpha1}$ radiation. Brunauer−Emmett−Teller (BET) surface area measurements were conducted on a Quadrasorb SI machine in N_2-adsorption mode. Samples were degassed at 150 °C for 15 h under vacuum prior to the measurements. Raman spectra were recorded on a Renishaw Ramascope spectrometer at 514 nm laser excitation. UV/vis diffuse reflectance absorption spectra were recorded on a Lambda 650 S PerkinElmer UV−visible spectrometer. XPS spectra were measured on an Axis Ultra DLD spectrometer (Kratos, Manchester, U.K.) with a 0.1 eV energy resolution. Measurements were performed with a monochromatic Al Kα source without any preceding sputter cleaning or other procedures that might alter the surface of the crystals. The C 1s peak at 284.6 eV was set as a reference for all XPS peak positions. The O 1s peaks were fitted with the XPSPEAK 4.1 software. Magnetic susceptibility measurements were conducted on a 7 T Quantum Design MPMS SQUID instrument at a magnetic field of 1.0 T in the temperature range 5−300 K in both heating and cooling modes. Solid-state ^{7}Li NMR spectra were recorded on a Bruker DRX-500 spectrometer modified for solid-state measurements with MAS sample spinning up to 15 kHz (4 mm rotors) and high-power 9.5 Hz decoupling. The NMR frequency was 194.41 MHz for ^{7}Li (I = 3/2, QM = 0.045). The composition of lithium cobalt oxides was analyzed with ICP-AES on an Optima 5300DV spectrometer with a 0.008 nm resolution. Samples were completely dissolved in nitric acid and diluted to concentration within the detection range of the spectrometer. The lithium content of $Li_{1-x}CoO_2$ after different delithiation times was determined by ICP-AES (Mikroanalytisches Labor Pascher, Remagen, Germany).

ASSOCIATED CONTENT

Supporting Information

The Supporting Information is available free of charge on the ACS Publications website at DOI: 10.1021/acscatal.5b00078.

SEM and TEM pictures for LT-/HT-$LiCoO_2$ and LT-/HT-$Li_{0.4}CoO_2$, FT-IR and UV/vis spectra, PXRD patterns, and photochemical water oxidation test results for LT-/HT-$LiCoO_2$ after different delithiation times (PDF)

AUTHOR INFORMATION

Corresponding Author

*E-mail for G.R.P.: greta.patzke@chem.uzh.ch.

Notes

The authors declare no competing financial interest.

ACKNOWLEDGMENTS

Financial support by the Swiss National Science Foundation (Sinergia Grant No. CRSII2_136205/1) is gratefully acknowledged. This work has been supported by the University Research Priority Program (URPP) for solar light to chemical energy conversion (LightChEC). H.L. thanks the China Scholarship Council for a Ph.D. fellowship. We thank Dr. Wolfram Lorenz (ETH Zurich) for magnetic susceptibility measurements and Dr. Ferdinand Wild (UZH) and Dr. Jörg Patscheider (EMPA Dübendorf) for XPS and other analytical measurements.

REFERENCES

(1) (a) Lewis, N. S.; Nocera, D. G. *Proc. Natl. Acad. Sci. U. S. A.* **2006**, *43*, 15729−15735. (b) Berardi, S.; Drouet, S.; Francàs, L.; Gimbert-Surinach, C.; Guttentag, M.; Richmond, C.; Stoll, T.; Llobet, A. *Chem. Soc. Rev.* **2014**, *43*, 7501−7519. (c) Swierk, J. R.; Mallouk, T. E. *Chem. Soc. Rev.* **2013**, *42*, 2357−2387. (d) Alibabaei, L.; Brennaman, M. K.; Norris, M. R.; Kalanyan, B.; Song, W.; Losego, M. D.; Concepcion, J.

DOI: 10.1021/acscatal.5b00078
ACS Catal. 2015, 5, 3791−3800

J.; Binstead, R. A.; Parsons, G. N.; Meyer, T. J. *Proc. Natl. Acad. Sci. U. S. A.* **2013**, *110*, 20008−20013. (e) Antonietti, M. *Angew. Chem., Int. Ed.* **2013**, *52*, 1086−1087.
(2) (a) Young, K. J.; Martini, L. A.; Milot, R. L.; Snoeberger, R. C., III; Batista, V. S.; Schmuttenmaer, C. A.; Crabtree, R. H.; Brudvig, G. W. *Coord. Chem. Rev.* **2012**, *256*, 2503−2520. (b) Sartorel, A.; Bonchio, M.; Campgna, S.; Scandola, F. *Chem. Soc. Rev.* **2013**, *42*, 2262−2280. (c) McAlpin, J. G.; Stich, T. A.; Casey, W. H.; Britt, R. D. *Coord. Chem. Rev.* **2012**, *256*, 2445−2452. (d) Singh, A.; Spiccia, L. *Coord. Chem. Rev.* **2013**, *257*, 2607−2622. (e) Zuccaccia, C.; Bellachioma, G.; Bortolini, O.; Bucci, A.; Savini, A.; Macchioni, A. *Chem. - Eur. J.* **2014**, *20*, 3446−3456. (f) Goberna-Ferrón, S.; Hernández, W. Y.; Rodríguez-García, B.; Galán-Mascarós, J. R. *ACS Catal.* **2014**, *4*, 1637−1641. (g) Duan, L.; Bozoglian, F.; Mandal, S.; Stewart, B.; Privalov, T.; Llobet, A.; Sun, L. *Nat. Chem.* **2012**, *4*, 418−423.
(3) (a) Crabtree, R. H. *Chem. Rev.* **2012**, *112*, 1536−1554. (b) Stracke, J. J.; Finke, R. G. *ACS Catal.* **2014**, *4*, 909−933. (c) Artero, V.; Fontecave, M. *Chem. Soc. Rev.* **2013**, *42*, 2338−2356.
(4) Zhang, M.; Respinis, M. d.; Frei, H. *Nat. Chem.* **2014**, *6*, 362−367.
(5) (a) Pokhrel, R.; Brudvig, G. W. *Phys. Chem. Chem. Phys.* **2014**, *16*, 11812−11821. (b) Cox, N.; Pantazis, D. A.; Neese, F.; Lubitz, W. *Acc. Chem. Res.* **2013**, *46*, 1588−1596. (c) Dau, H.; Zaharieva, I.; Haumann, M. *Curr. Opin. Chem. Biol.* **2012**, *16*, 3−10.
(6) (a) Tsui, E. Y.; Agapie, T. *Proc. Natl. Acad. Sci. U. S. A.* **2013**, *110*, 10084−10088. (b) Mukherjee, S.; Stull, J. A.; Yano, J.; Stamatatos, T. C.; Pringouri, K.; Stich, T. A.; Abboud, K. A.; Britt, R. D.; Yachandra, V. K.; Christou, G. *Proc. Natl. Acad. Sci. U. S. A.* **2012**, *109*, 2257−2262. (c) Shevchenko, D.; Anderlund, M. F.; Styring, S.; Dau, H.; Zaharieva, I.; Thapper, A. *Phys. Chem. Chem. Phys.* **2014**, *16*, 11965−11975.
(7) (a) McCool, N. S.; Robinson, D. M.; Sheats, J. E.; Dismukes, G. C. *J. Am. Chem. Soc.* **2011**, *133*, 11446−11449. (b) Zhang, B.; Li, F.; Yu, F.; Wang, X.; Zhou, X.; Li, H.; Jiang, Y.; Sun, L. *ACS Catal.* **2014**, *4*, 804−809. (c) Berardi, S.; Ganga, G. L.; Natali, M.; Bazzan, I.; Puntoriero, F.; Sartorel, A.; Scandola, F.; Campagna, S.; Bonchio, M. *J. Am. Chem. Soc.* **2012**, *134*, 11104−11107. (d) Smith, P. F.; Kaplan, C.; Sheats, J. E.; Robinson, D. M.; McCool, N. S.; Mezle, N.; Dismukes, G. C. *Inorg. Chem.* **2014**, *53*, 2113−2121. (e) Kuznetsov, A. E.; Geletii, Y. V.; Hill, C. L.; Musaev, D. G. *J. Phys. Chem. A* **2010**, *114*, 11417−11424. (f) Xu, Z.; Li, F.; Li, H.; Zhang, B.; Yu, F.; Sun, L. *ChemSusChem* **2014**, *7*, 2453−2456. (g) Ganga, G. L.; Nardo, V. M.; Cordaro, M.; Natali, M.; Vitale, S.; Licciardello, A.; Nastasi, F.; Campagna, S. *Dalton Trans.* **2014**, *43*, 14926−14930. (h) Evangelisti, F.; Güttinger, R.; Moré, R.; Luber, S.; Patzke, G. R. *J. Am. Chem. Soc.* **2013**, *135*, 18734−18737. (i) Gao, Y.; Crabtree, R. H.; Brudvig, G. W. *Inorg. Chem.* **2012**, *51*, 4043−4050.
(8) (a) Robinson, D. M.; Go, Y. B.; Greenblatt, M.; Dismukes, G. C. *J. Am. Chem. Soc.* **2010**, *132*, 11467−11469. (b) Gardner, G. P.; Go, Y. B.; Robinson, D. M.; Smith, P. F.; Hadermann, J.; Abakumov, A.; Greenblatt, M.; Dismukes, G. C. *Angew. Chem., Int. Ed.* **2012**, *51*, 1616−1619. (c) Iyer, A.; Del-Pilar, J.; King'ondu, C. K.; Kissel, E.; Garces, H. F.; Huang, H.; El-Sawy, A. M.; Dutta, P. K.; Suib, S. L. *J. Phys. Chem. C* **2012**, *116*, 6474−6483. (d) Najafpour, M. M.; Ehrenberg, T.; Wiechen, M.; Kurz, P. *Angew. Chem., Int. Ed.* **2010**, *49*, 2233−2237. (e) Wiechen, M.; Zaharieva, I.; Dau, H.; Kurz, P. *Chem. Sci.* **2012**, *3*, 2330−2339. (f) Jin, K.; Park, J.; Lee, J.; Yang, K.; Pardhan, G. K.; Sim, U.; Jeong, D.; Jang, H. L.; Park, S.; Kim, D.; Sung, N.-E.; Kim, S. H.; Han, S.; Nan, K. T. *J. Am. Chem. Soc.* **2014**, *136*, 7435−7443. (g) Boppana, V. B. R.; Yusuf, S.; Hutchings, G. S.; Jiao, F. *Adv. Funct. Mater.* **2013**, *23*, 878−884. (h) Hong, D.; Yamada, Y.; Nomura, A.; Fukuzumi, S. *Phys. Chem. Chem. Phys.* **2013**, *15*, 19125−19128. (i) Hocking, R. K.; Brimblecombe, R.; Chang, L.-Y.; Singh, A.; Cheah, M. H.; Glover, C.; Casey, W. H.; Spiccia, L. *Nat. Chem.* **2011**, *3*, 461−466.
(9) (a) Han, X.-B.; Zhang, Z.-M.; Zhang, T.; Li, Y.-G.; Lin, W.; You, W.; Su, Z.-M.; Wang, E.-B. *J. Am. Chem. Soc.* **2014**, *136*, 5359−5366. (b) Yin, Q. S.; Tan, J. M.; Besson, C.; Geletii, Y. V.; Musaev, D. G.; Kuznetsov, A. E.; Luo, Z.; Hardcastle, K. I.; Hill, C. L. *Science* **2010**, *328*, 342−345. (c) Lv, H.; Song, J.; Geletii, Y. V.; Vickers, J. W.; Sumliner, J. M.; Musaev, D. G.; Kögerler, P.; Zhuk, P. F.; Bacsa, J.; Zhu, G.; Hill, C. L. *J. Am. Chem. Soc.* **2014**, *136*, 9268−9271. (d) Al-Oweini, R.; Sartorel, A.; Bassil, B. S.; Natali, M.; Berardi, S.; Scandola, F.; Kortz, U.; Bonchio, M. *Angew. Chem., Int. Ed.* **2014**, *53*, 11182−11185.
(10) Swiegers, G. F.; Clegg, J. K.; Stranger, R. *Chem. Sci.* **2011**, *2*, 2254−2262.
(11) Kanan, M. W.; Nocera, D. G. *Science* **2008**, *321*, 1072−1075.
(12) (a) Smith, R. D. L.; Prévot, M. S.; Fagan, R. D.; Zhang, Z.; Sedach, P. A.; Siu, M. K. J.; Trudel, S.; Berlinguette, C. P. *Science* **2013**, *340*, 60−63. (b) Rish, M.; Klingan, K.; Rigleb, F.; Chernev, P.; Zaharieva, I.; Fischer, A.; Dau, H. *ChemSusChem* **2012**, *5*, 542−549. (c) Indra, A.; Menezes, P.; Zaharieva, I.; Baktash, E.; Pfrommer, J.; Schwarze, M.; Dau, H.; Driess, M. *Angew. Chem., Int. Ed.* **2013**, *52*, 13206−13210. (d) Kuai, L.; Geng, J.; Chen, C.; Kan, E.; Liu, Y.; Wang, Q.; Geng, B. *Angew. Chem., Int. Ed.* **2014**, *53*, 7547−7551.
(13) (a) Risch, M.; Khare, V.; Zaharieva, L.; Gerencser, L.; Dau, H. *J. Am. Chem. Soc.* **2009**, *131*, 6936−6937. (b) Kanan, M. W.; Yano, J.; Surendranath, Y.; Dincă, M.; Yachandra, V. K.; Nocera, D. G. *J. Am. Chem. Soc.* **2010**, *132*, 13692−13701. (c) Gerken, J. B.; McAlpin, J. G.; Chen, J. Y. C.; Rigsby, M. L.; Casey, W. H.; Britt, R. D.; Stahl, S. S. *J. Am. Chem. Soc.* **2011**, *133*, 14431−14442.
(14) (a) Zidki, T.; Zhang, L.; Shafirovich, V.; Lymar, S. V. *J. Am. Chem. Soc.* **2012**, *134*, 14275−14278. (b) Kim, S. J.; Lee, Y.; Lee, D. K.; Lee, J. W.; Kang, J. K. *J. Mater. Chem. A* **2014**, *2*, 4136−4139. (c) Subbraman, R.; Tripkovic, D.; Chang, K.-C.; Strmcnik, D.; Paulikas, A. P.; Hirunsit, P.; Chan, M.; Greeley, J.; Stamenkovic, V.; Markovic, N. M. *Nat. Mater.* **2012**, *11*, 550−557.
(15) Ullman, A. M.; Liu, Y.; Huynh, M.; Bediako, D. K.; Wang, H.; Anderson, B. L.; Powers, D. C.; Breen, J. J.; Abruna, H. D.; Nocera, D. G. *J. Am. Chem. Soc.* **2014**, *136*, 17681−17688.
(16) (a) Maiyalagan, T.; Jarvis, K. A.; Soosairaj, T.; Ferreira, P. J.; Manthiram, A. *Nat. Commun.* **2014**, *5*, 3949. (b) Lu, Z.; Wang, H.; Kong, D.; Yan, Y.; Hsu, P.-C.; Zheng, G.; Yao, H.; Liang, Z.; Sun, X.; Cui, Y. *Nat. Commun.* **2014**, *5*, 4345.
(17) Lee, S. W.; Carlton, C.; Risch, M.; Surendranath, Y.; Chen, S.; Furutsuki, A.; Yamada, A.; Nocera, D. G.; Shao-Horn, Y. *J. Am. Chem. Soc.* **2012**, *134*, 16959−16962.
(18) Indra, A.; Menezes, P. W.; Sahraie, N. R.; Bergmann, A.; Das, C.; Tallarida, M.; Schmei*ß*er, D.; Strasser, P.; Driess, M. *J. Am. Chem. Soc.* **2014**, *136*, 17530−17536.
(19) Porthault, H.; Baddour-Hadjeanc, R.; Cras, F. L.; Bourbon, C.; Franger, S. *Vib. Spectrosc.* **2012**, *62*, 152−158.
(20) Huang, W.; Frech, R. *Solid State Ionics* **1996**, *86*−*88*, 395−400.
(21) Valkeapää, M.; Katsumata, Y.; Asako, I.; Motohashi, T.; Chan, T. S.; Liu, R. S.; Chen, J. M.; Yamauchi, H.; Karppinen, M. *J. Solid State Chem.* **2007**, *180*, 1608−1615.
(22) Nobili, F.; Dsoke, S.; Minicucci, M.; Croce, F.; Marassi, R. *J. Phys. Chem. B* **2006**, *110*, 11310−11313.
(23) Chebiam, R. V.; Prado, F.; Manthiram, A. *Chem. Mater.* **2001**, *13*, 2951−2957.
(24) (a) Jiao, F.; Frei, H. *Angew. Chem., Int. Ed.* **2009**, *48*, 1841−1844. (b) Yang, C.-C.; Eggenhuisen, T. M.; Wolters, M.; Agiral, A.; Frei, H.; Jongh, P. E.; Jong, K. P.; Mul, G. *ChemCatChem* **2013**, *5*, 550−556. (c) Rosen, J.; Hutchings, G. S.; Jiao, F. *J. Am. Chem. Soc.* **2013**, *135*, 4516−4521. (d) Grzelczak, M.; Zhang, J.; Pfrommer, J.; Hartmann, J.; Driess, M.; Antonietti, M.; Wang, X. *ACS Catal.* **2013**, *3*, 383−388. (e) Blakemore, J. D.; Gray, H. B.; Winkler, J. R.; Müller, A. M. *ACS Catal.* **2013**, *3*, 2497−2500. (f) Ahn, H. S.; Yano, J.; Tilley, T. D. *Energy Environ. Sci.* **2013**, *6*, 3080−3087.
(25) Liu, H.; Patzke, G. R. *Chem. - Asian J.* **2014**, *9*, 2249−2259.
(26) (a) Vickers, J. W.; Lv, H.; Sumliner, J. M.; Zhu, G.; Luo, Z.; Musaev, D. G.; Geletii, Y. V.; Hill, C. L. *J. Am. Chem. Soc.* **2013**, *135*, 14110−14118. (b) Stracke, J. J.; Finke, R. G. *J. Am. Chem. Soc.* **2011**, *133*, 14872−14875.
(27) (a) May, K. J.; Carlton, C. E.; Stoerzinger, K. A.; Risch, M.; Suntivich, J.; Lee, Y.-L.; Grimaud, A.; Shao-Horn, Y. *J. Phys. Chem. Lett.*

DOI: 10.1021/acscatal.5b00078
ACS Catal. 2015, 5, 3791−3800

2012, *3*, 3264−3270. (b) Grimaud, A.; May, K. J.; Carlton, C. E.; Lee, Y.-L.; Risch, M.; Hong, W. T.; Zhou, J.; Shao-Horn, Y. *Nat. Commun.* **2013**, *4*, 2439.
(28) Levasseur, S.; Ménétrier, M.; Shao-Horn, Y.; Gautier, L.; Audemer, A.; Demazeau, G.; Largeteau, A.; Delmas, C. *Chem. Mater.* **2003**, *15*, 348−354.
(29) Appapillai, A. T.; Mansour, A. N.; Cho, J.; Shao-Horn, Y. *Chem. Mater.* **2007**, *19*, 5748−5757.
(30) (a) Yoon, W.-S.; Kim, K.-B.; Kim, M.-G.; Lee, M.-K.; Shin, H.-J.; Lee, J.-M.; Yo, C.-H. *J. Phys. Chem. B* **2002**, *106*, 2526−2532. (b) Aydinol, M. K.; Kohan, A. F.; Ceder, G.; Cho, K.; Joannopoulos, J. *Phys. Rev. B: Condens. Matter Mater. Phys.* **1997**, *56*, 1354−1365. (c) Galakhov, V. R.; Neumann, M.; Kellerman, D. G. *Appl. Phys. A: Mater. Sci. Process.* **2009**, *94*, 497−500.
(31) (a) Takahashi, Y.; Kijima, N.; Tokiwa, K.; Watanabe, T.; Akimoto, J. *J. Phys.: Condens. Matter* **2007**, *19*, 436202. (b) Takahashi, Y.; Gotoh, Y.; Akimoto, J.; Mizuta, S.; Tokiwa, K.; Watanabe, T. *J. Solid State Chem.* **2002**, *164*, 1−4.
(32) Han, B.; Qian, D.; Risch, M.; Chen, H.; Chi, M.; Meng, Y. S.; Shao-Horn, Y. *J. Phys. Chem. Lett.* **2015**, *6*, 1357−1362.
(33) Stoerzinger, K. A.; Choi, W. S.; Jeen, H.; Lee, H. N.; Shao-Horn, Y. *J. Phys. Chem. Lett.* **2015**, *6*, 487−492.
(34) (a) Hatakeyama, M.; Nakata, H.; Wakabayashi, M.; Yokojima, S.; Nakamura, S. *J. Phys. Chem. A* **2012**, *116*, 7089−7097. (b) Mattioli, G.; Giannozzi, P.; Bonapasta, A. A.; Guidoni, L. *J. Am. Chem. Soc.* **2013**, *135*, 15353−15363. (c) Zhang, M.; de Respinis, M.; Frei, H. *Nat. Chem.* **2014**, *6*, 362. (d) Li, X.; Siegbahn, P. E. M. *J. Am. Chem. Soc.* **2013**, *135*, 13804−13813.
(35) (a) Xiang, X.; Fielden, J.; Rodriguez-Cordoba, W. E.; Huang, Z.; Zhang, N.; Luo, Z.; Musaev, D. G.; Lian, T.; Hill, C. L. *J. Phys. Chem. C* **2013**, *117*, 918−926. (b) Soo, H. S.; Agiral, A.; Bachmeier, A.; Frei, H. *J. Am. Chem. Soc.* **2012**, *134*, 17104−17116. (c) Agiral, A.; Soo, H. S.; Frei, H. *Chem. Mater.* **2013**, *25*, 2264−2273.

DOI: 10.1021/acscatal.5b00078
ACS Catal. 2015, 5, 3791−3800